The mechanistic basis of both deep and durable antitumor activity by combinatorial inhibition of MAT2A and PRMT5 in MTAP$^{-/-}$ tumors

Damien Garbett, Arjun A. Rao, Marcus M. Fischer, Brian Belmontes[1], Katherine Slemmons[1], Mason J. Appel, Zhipeng Fang, Parker Y. Jameson, Angelica Gonzalez-Sanchez, Rebeca M. Choy, Scott R. Tyler, John Vivian, J. Carl Schultz, Yevgeniy Freyman, Khristina Magallanes, Pari Lanham, Atul Rathore, Natalie Bresnahan, Austin Li, Oscar Aubi, Kai Yang, Ivan Shabalin, Kelly Trego, Briana Marinoni, Christian R. Frey, Yuchen Bai, Paul E. Hughes[1], Peter Teriete, Michael A. White, Claire L. Neilan IDEAYA Biosciences, Inc., South San Francisco, CA, USA, [1]Amgen, Thousand Oaks, CA, USA

Overview

MTAP is frequently deleted in cancer, causing loss of 1-carbon salvage and the accumulation of the metabolite MTA.

MTAP$^{-/-}$ tumors require sufficient MAT2A activity to support the methionine cycle and to ameliorate direct inhibition of the essential methyltransferase, PRMT5, by MTA; nominating MAT2A inhibition as a therapeutic opportunity.

Further, MTA-cooperative PRMT5 inhibitors (PRMT5i^{MTA}) can exploit MTA accumulation by binding directly to a PRMT5-MTA complex.

IDE397 (MAT2Ai) and AMG 193 (PRMT5i^{MTA}) were independently developed to selectively target MTAP$^{-/-}$ tumors and have demonstrated monotherapy activity in the clinic (ref 1).

Codependent MAT2A and PRMT5 biology prompted focused evaluation of MAT2Ai/PRMT5i^{MTA} combination.

IDE397 and AMG 193 show significant, well tolerated, preclinical combination benefit for both the depth and durability of anti-tumor responses, including complete regressions that are sustained off-treatment.

Direct assessment of PRMT5 target engagement indicated that IDE397 selectively augmented PRMT5i^{MTA} activity in MTAP$^{-/-}$ cells via elevation of MTA/SAM molar ratios.

CRISPR KO screens identified modulators of sensitivity to IDE397 or PRMT5i^{MTA} that were predominantly but not entirely overlapping; indicating both common and distinct biology associated with each agent.

Resistance to the combination in culture was primarily a consequence of disrupted polyamine biosynthesis, a bypass mechanism unlikely to operate in tumors due to dependency on polyamines for growth and survival.

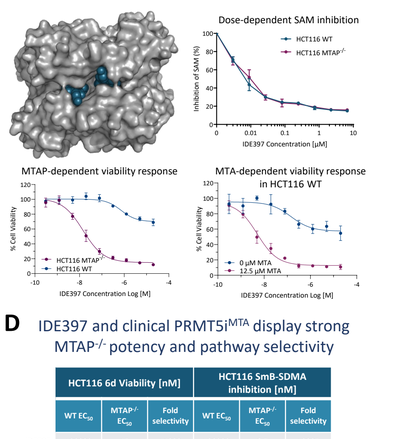
Transcript profiling of relapsed CDX tumors from single agent treatment arms revealed distinct and complementary monotherapy mechanisms that deliver durable antitumor activity in combination.

As expected, PDX profiling demonstrated robust IDE397/AMG 193 combination benefit in multiple indications.

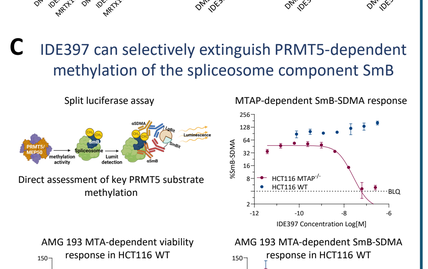
These findings support clinical evaluation of the IDE397/AMG 193 combination (NCT05975073).

Fig 1. MAT2A and PRMT5 buttress both shared and distinct biological vulnerabilities in MTAP$^{-/-}$ cancer cells

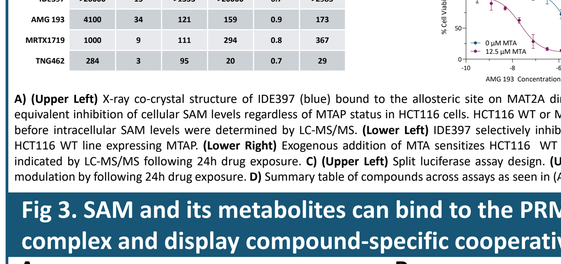
A MTAP and MAT2A are key nodes within a metabolic system vital for tumor growth and survival



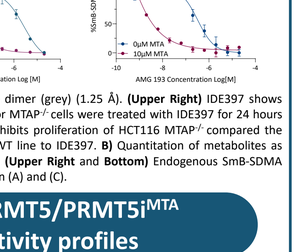
B MAT2A and PRMT5 share top RNAi co-dependency relationships within the CCLE



C MAT2A and PRMT5 codependency networks indicate both shared and distinct MOAs



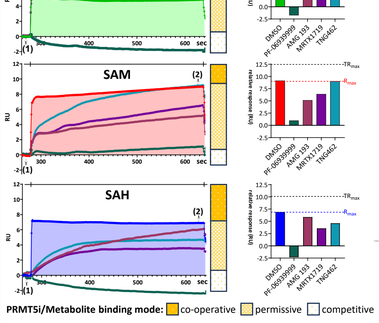
D MTA accumulation upon MTAP loss is a function of both synthesis and export



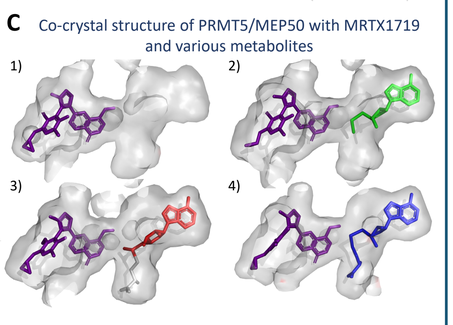
A) Schematic of one-carbon cycle. **B)** Top 100 RNAi dependency correlations with PRMT5 **(Left)** and MAT2A **(Right)**; highlighted are PRMT5 and its adapter proteins as well as other PRMTs, methyltransferases and splicing components. **C)** Positively associated GSEA pathway analysis of genes whose dependencies were correlated with both MAT2A and PRMT5 **(Left)**, or differentially correlated with either MAT2A **(Center)**, or PRMT5 **(Right)**, indicating aspects of shared tumor vulnerabilities as well as unique components of MAT2A or PRMT5 vulnerabilities. **D)** Quantitative MTA assessment by LC-MS/MS.

Fig 2. IDE397 can elevate MTA/SAM ratios selectively in MTAP$^{-/-}$ cells to suppress PRMT5 activity below threshold required for tumor cell viability

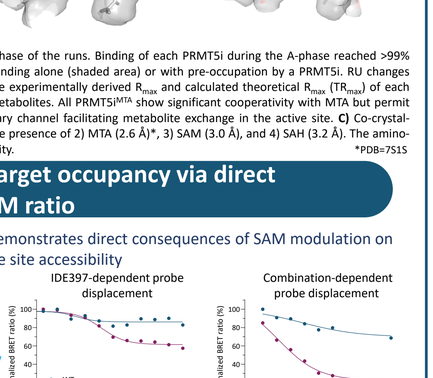
A IDE397 is an allosteric MAT2A inhibitor with a maximum SAM inhibition limit that supports MTAP wild-type cell function



B IDE397 exposure is sufficient to amplify MTA/SAM ratios in MTAP$^{-/-}$ cells without perturbing MTA accumulation



C IDE397 can selectively extinguish PRMT5-dependent methylation of the spliceosome component SmB



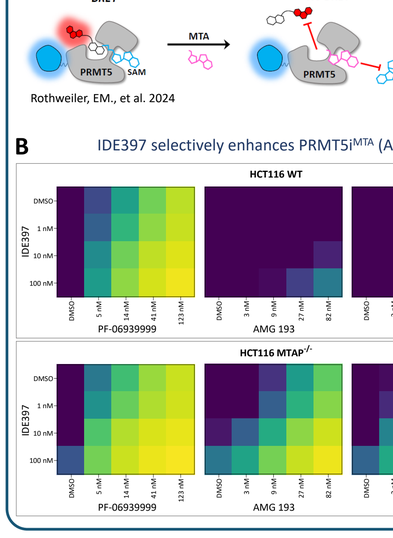
D IDE397 and clinical PRMT5i^{MTA} display strong MTAP$^{-/-}$ potency and pathway selectivity

	HCT116 6d Viability [nM]			HCT116 SmB-SDMA inhibition [nM]		
	WT EC_{50}	MTAP$^{-/-}$ EC_{50}	Fold selectivity	WT EC_{50}	MTAP$^{-/-}$ EC_{50}	Fold selectivity
IDE397	>20000	15	>1333	>20000	6.7	>2985
AMG 193	4100	34	121	159	0.9	173
MRTX1719	1000	9	111	294	0.8	367
TNG462	284	3	95	20	0.7	29

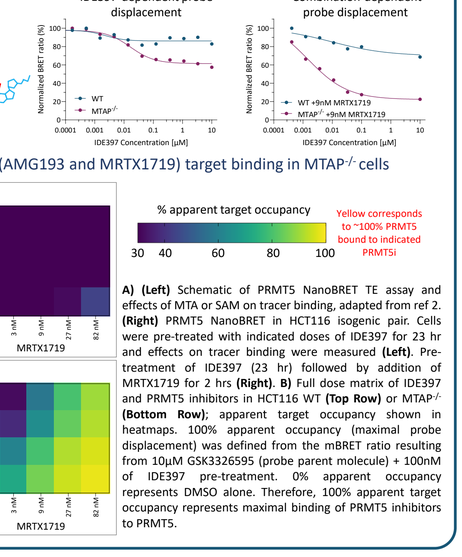
A) (Upper Left) X-ray co-crystal structure of IDE397 (blue) bound to the allosteric site on MAT2A dimer (grey) (1.25 Å). **(Upper Right)** IDE397 shows equivalent inhibition of cellular SAM levels regardless of MTAP status in HCT116 cells. HCT116 WT or MTAP$^{-/-}$ cells were treated with IDE397 for 24 hours before intracellular SAM levels were determined by LC-MS/MS. **(Lower Left)** IDE397 selectively inhibits proliferation of HCT116 MTAP$^{-/-}$ compared the HCT116 WT line expressing MTAP. **(Lower Right)** Exogenous addition of MTA sensitizes HCT116 WT line to IDE397. **B)** Quantitation of metabolites as indicated by LC-MS/MS following 24h drug exposure. **C) (Upper Left)** Split luciferase assay design. **(Upper Right** and **Bottom)** Endogenous SmB-SDMA modulation by following 24h drug exposure. **D)** Summary table of compounds across assays as seen in (A) and (C).

Fig 3. SAM and its metabolites can bind to the PRMT5/PRMT5i^{MTA} complex and display compound-specific cooperativity profiles

A ABA-type SPR data shows binding of SAM and its metabolites in the presence of PRMT5i^{MTA}



B Metabolite access to the substrate binding pocket through a potential secondary channel



C Co-crystal structure of PRMT5/MEP50 with MRTX1719 and various metabolites

A) Schematic of ABA-experimental layout and sensorgrams from the B-phase of the runs. Binding of each PRMT5i during the A-phase reached >99% occupancy (data not shown). B-phase binding curves show metabolite binding alone (shaded area) or with pre-occupation by a PRMT5i. RU changes between points (1) and (2) are shown as bar charts and compared to the experimentally derived R_{max} and calculated theoretical R_{max} (TR_{max}) of each metabolite. The SAM-competitive PF-06939999 prevents binding of all metabolites. All PRMT5i^{MTA} show significant cooperativity with MTA but permit lower affinity binding of SAM and SAH. **B)** Cartoon of potential secondary channel facilitating metabolite exchange in the active site. **C)** Co-crystal-structures of 1) MRTX1719 (1.9 Å) in the PRMT5 binding pocket, and in the presence of 2) MTA (2.6 Å)*, 3) SAM (3.0 Å), and 4) SAH (3.2 Å). The amino-acid tail of SAM, shown in grey, was not fully resolved in the electron density. *PDB=7S1S

Fig 4. IDE397 magnifies PRMT5i^{MTA} target occupancy via direct optimization of the cellular MTA/SAM ratio

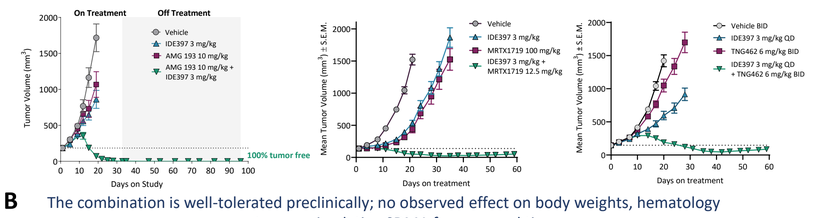
A SAM cooperative PRMT5 target occupancy probe demonstrates direct consequences of SAM modulation on PRMT5 active site accessibility

B IDE397 selectively enhances PRMT5i^{MTA} (AMG193 and MRTX1719) target binding in MTAP$^{-/-}$ cells

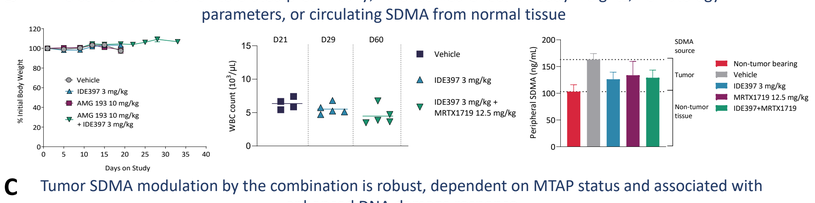
A) (Left) Schematic of PRMT5 NanoBRET TE assay and effects of MTA or SAM on tracer binding, adapted from ref 2. **(Right)** PRMT5 NanoBRET in HCT116 isogenic pair. Cells were pre-treated with indicated doses of IDE397 for 23 hr and effects on tracer binding were measured **(Left)**. Pre-treatment of IDE397 (23 hr) followed by addition of MRTX1719 for 2 hrs **(Right)**. **B)** Full dose matrix of IDE397 and PRMT5 inhibitors in HCT116 WT **(Top Row)** or MTAP$^{-/-}$ **(Bottom Row)**; apparent target occupancy shown in heatmaps. 100% apparent occupancy (maximal probe displacement) was defined from the mBRET ratio resulting from 10µM GSK3326595 (probe parent molecule) + 100nM of IDE397 pre-treatment. 0% apparent occupancy represents DMSO alone. Therefore, 100% apparent target occupancy represents maximal binding of PRMT5 inhibitors to PRMT5.

Fig 5. IDE397 in combination with clinical PRMT5i^{MTA} inhibitors is well tolerated and delivers deep and durable MTAP$^{-/-}$ tumor regressions

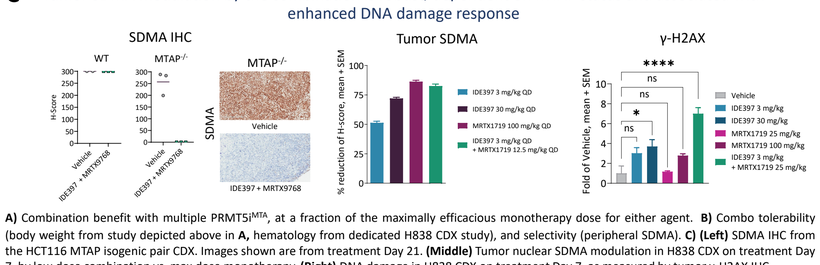
A The combination of PRMT5i^{MTA} and IDE397 produces deep and sustained regression in the NSCLC CDX model NCI-H838, regardless of PRMT5i^{MTA} chemotype used



B The combination is well-tolerated preclinically; no observed effect on body weights, hematology parameters, or circulating SDMA from normal tissue



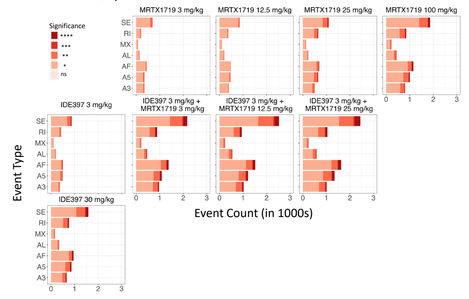
C Tumor SDMA modulation by the combination is robust, dependent on MTAP status and associated with enhanced DNA damage response



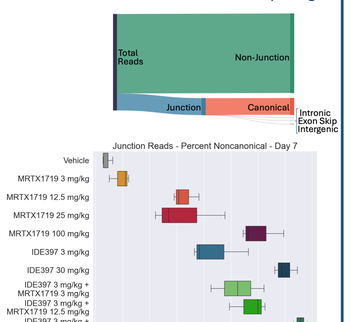
A) Combination benefit with multiple PRMT5i^{MTA}, at a fraction of the maximally efficacious monotherapy dose for either agent. **B)** Combo tolerability (body weight from study depicted above in **A,** hematology from dedicated H838 CDX study), and selectivity (peripheral SDMA). **C) (Left)** SDMA IHC from the HCT116 MTAP isogenic pair CDX. Images shown are from treatment Day 21. **(Middle)** Tumor nuclear SDMA modulation in H838 CDX on treatment Day 7, by low dose combination vs. max dose monotherapy. **(Right)** DNA damage in H838 CDX on treatment Day 7, as measured by tumor γ-H2AX IHC.

Fig 6. Allosteric inhibition of MAT2A delivers highly selective perturbation of SAM-dependent biological systems

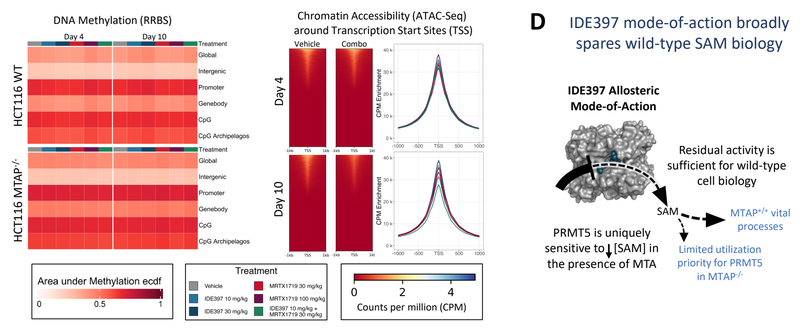
A Assessment of pre-mRNA splicing *in vivo* in MTAP$^{-/-}$ NSCLC indicates strong perturbation by mono- and combination therapy



B InExplorer reveals extensive drug-induced non-canonical splicing

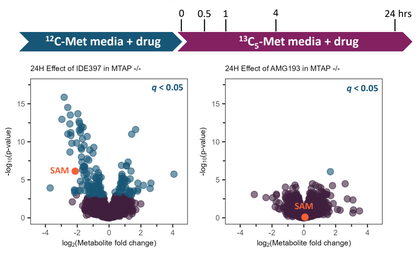


C DNA methylation and chromatin accessibility profiles are not globally affected by IDE397 or PRMT5i^{MTA} *in vivo*

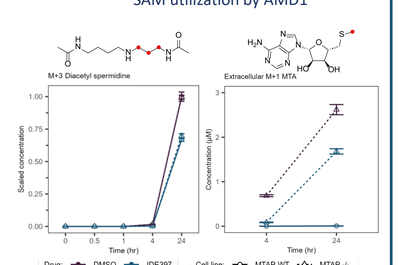


D IDE397 mode-of-action broadly spares wild-type SAM biology

E Extensive metabolic reprogramming is observed selectively with IDE397 versus PRMT5i^{MTA}



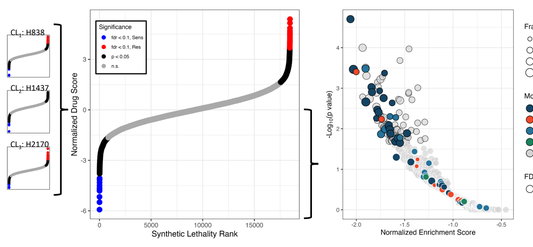
F MTA synthesis is maintained- indicating priority SAM utilization by AMD1



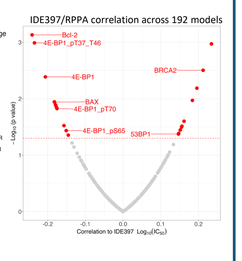
A) The indicated tumor samples were collected on treatment Day 7 from an H838 CDX PKPD study and analyzed by RNA-Seq. Alternative pre-mRNA splicing events were quantified with SUPPA2 (ref 3). **SE**: skipped exon; **RI:** retained intron; **MX**: mutually exclusive exons; **AL**: alternative last exons; **AF**: alternative first exons; **A5**: alternative 5′ splice site events; **A3**: alternative 3′ splice site events. **B)** Noncanonical splicing events in (A) were quantified by InExplorer, a tool that uses decision trees to categorize junction reads. **C)** HCT116 MTAP isogenic pair CDX tumors were collected on treatment Day 4 and Day 10 and Reduced-Representation Bisulfite Sequencing (RRBS) or Assay for Transposase-Accessible Chromatin Sequencing (ATAC-Seq) was preformed to assess drug effects on global DNA methylation and chromatin respectively. **D)** Schematic indicating biological consequence of allosteric MAT2A inhibition. **E)** Global metabolite abundance and Met-adjacent carbon-13 metabolic flux were analyzed by mass-spectrometry in the HCT116 isogenic pair. At 24 hours in MTAP$^{-/-}$ cells, IDE397 significantly altered cellular levels of ~100 metabolites including SAM, while AMG 193 has a minimal affect on metabolite profile. **F)** Excretion of M+1 MTA and cellular M+3 Diacetyl spermidine at 4 and 24 hours are shown as proxies of polyamine synthesis rates. In MTAP$^{-/-}$ cells, IDE397 treatment minimally affected the rate of polyamine synthesis, and the cells continued to excrete accumulated MTA at high rates.

Fig 7. Pan-genomic evaluation of drug/gene interactions reveals shared and unique mechanistic modifiers of mono and combo drug responses

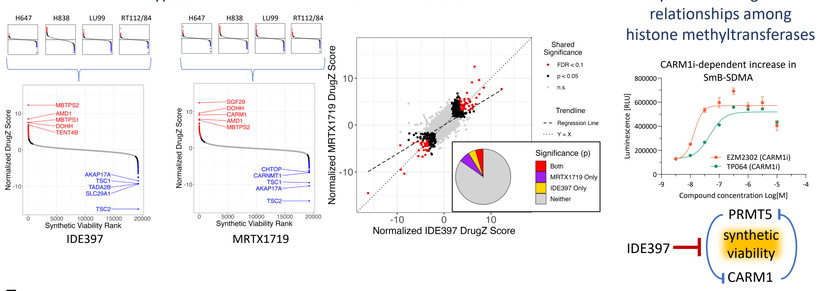
A CRISPR "sensitizer" screens across MTAP$^{-/-}$ models indicate DDR, one-carbon cycle, and mTOR pathway activity as key determinants of IDE397 response



B Molecular feature association concordance with FG data

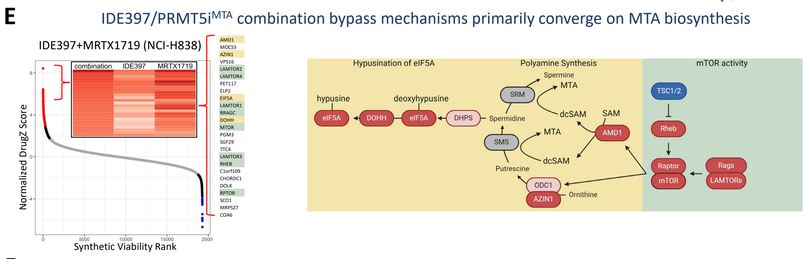


C CRISPR "resistor" screens across MTAP$^{-/-}$ models indicate shared and distinct bypass mechanisms for PRMT5i^{MTA} versus IDE397

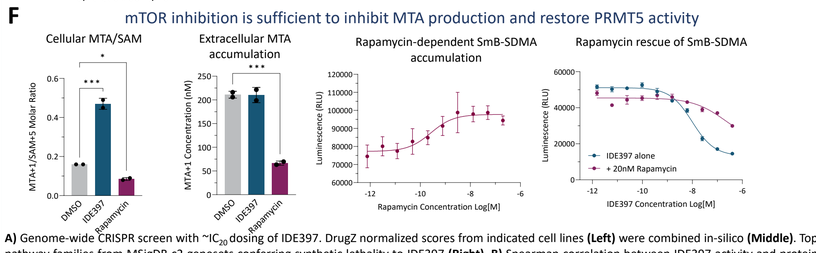


D PRMT5i^{MTA}-specific bypass may reflect antagonistic relationships among histone methyltransferases

E IDE397/PRMT5i^{MTA} combination bypass mechanisms primarily converge on MTA biosynthesis



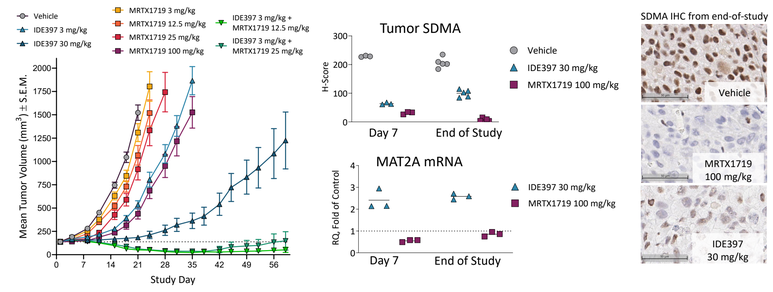
F mTOR inhibition is sufficient to inhibit MTA production and restore PRMT5 activity



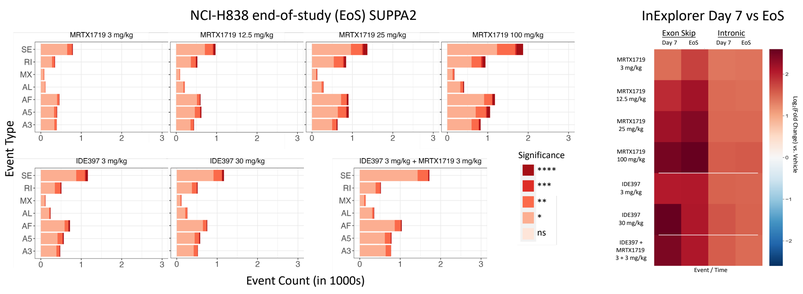
A) Genome-wide CRISPR screen with ~IC_{20} dosing of IDE397. DrugZ normalized scores from indicated cell lines **(Left)** were combined in-silico **(Middle)**. Top pathway families from MSigDB c2 genesets conferring synthetic lethality to IDE397 **(Right)**. **B)** Spearman correlation between IDE397 activity and protein expression from the DepMap RPPA dataset. **C)** Genome-wide CRISPR screen with IC_{30} dosing of IDE397 or MRTX1719. Normalized DrugZ scores from combined data from 4 cell lines was used to compare drug effects. **D)** Assays performed as in Figure 2B with CARM1 inhibitors (refs 4,5). **E)** Synthetic viability rank plot from NCI-H838 with IC_{20} of IDE397:MTRX1719 and heatmap of top 25 features across arms **(Left).** Mechanistic schematic **(Right)**. **F)** Assays performed in NCI-H838 cells with indicated compounds similar to those described in Figure 2B,C; MTA/SAM measurements were performed after 4 hr pulse of $^{13}C_5$-labeled methionine.

Fig 8. Combination therapy intercepts monotherapy acquired resistance mechanisms to deliver durable tumor regressions

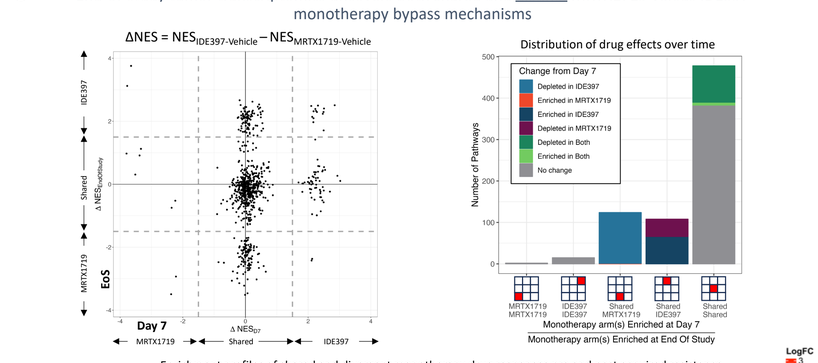
A PRMT5 and MAT2A modulation is maintained in tumors that become refractory to monotherapy PRMT5i^{MTA} or IDE397 in the NSCLC CDX model NCI-H838



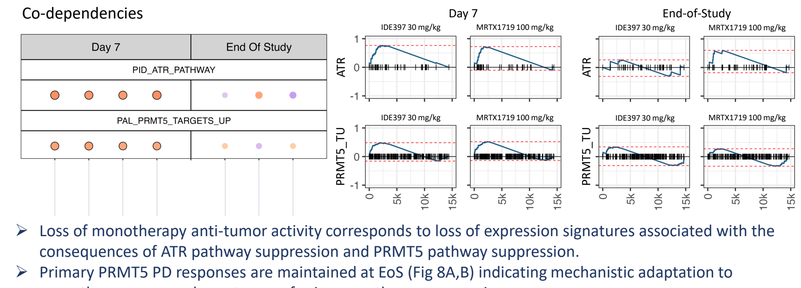
B pre-mRNA splicing analysis in relapsed tumors indicates continued strong perturbation by PRMT5i^{MTA}



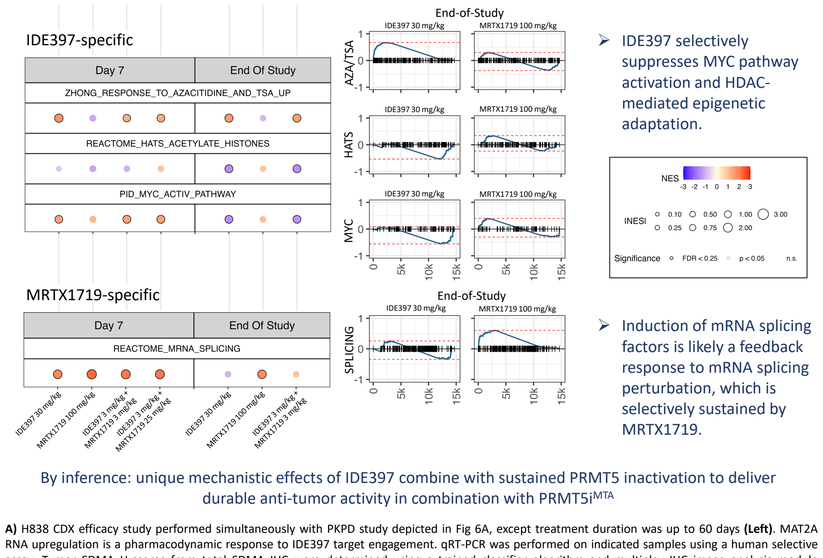
C End-of-study tumor transcriptomics uncovers both shared and distinct MRTX1719 versus IDE397 monotherapy bypass mechanisms



Co-dependencies



- Loss of monotherapy anti-tumor activity corresponds to loss of expression signatures associated with the consequences of ATR pathway suppression and PRMT5 pathway suppression.
- Primary PRMT5 PD responses are maintained at EoS (Fig 8A,B) indicating mechanistic adaptation to monotherapy occurs downstream of primary pathway suppression.



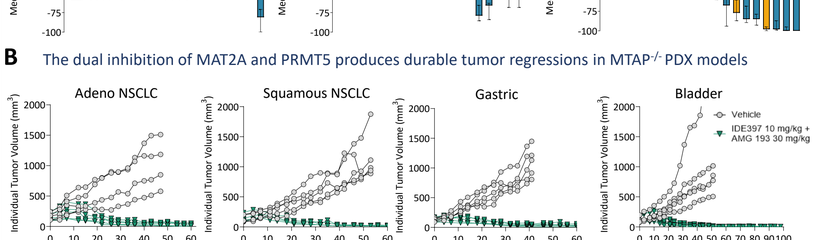
- IDE397 selectively suppresses MYC pathway activation and HDAC-mediated epigenetic adaptation.
- Induction of mRNA splicing factors is likely a feedback response to mRNA splicing perturbation, which is selectively sustained by MRTX1719.

By inference: unique mechanistic effects of IDE397 combine with sustained PRMT5 inactivation to deliver durable anti-tumor activity in combination with PRMT5i^{MTA}

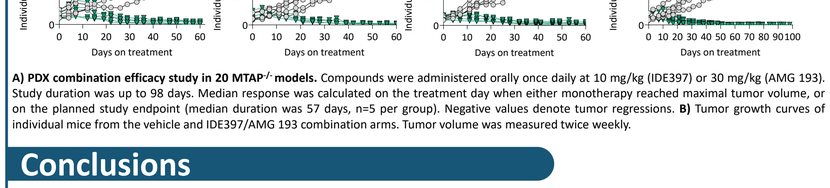
A) H838 CDX efficacy study performed simultaneously with PKPD study depicted in Fig 6A, except treatment duration was up to 60 days **(Left)**. MAT2A RNA upregulation is a pharmacodynamic response to IDE397 target engagement. qRT-PCR was performed on indicated samples using a human selective assay. Tumor SDMA H-scores from total SDMA IHC were determined using a trained classifier algorithm and multiplex IHC image analysis module **(Middle)**. Representative images are shown at 40x magnification **(Right)**. **B)** SUPPA2 identified alternative splicing distribution as a function of treatment dose at the End of Study (EOS), similar to Fig 6A. **C)** InExplorer quantified log fold changes in treatment vs. vehicle for Exon Skip and Intronic events. **C)** Normalized enrichment scores (NES) of IDE397 and MRTX1719 at maximum efficacious doses were identified using fgsea. Correlation between the difference in NES of IDE397 – MRTX1719 at EOS vs Vehicle is shown **(Top Left)** with a bar plot of frequency of event shared and distinct between the treatment timepoints **(Top Right)**. A heatmap of NES describes the magnitude **(Middle),** effect size and significance of key biological pathways **(Bottom**, all NES plots share identical x- and y-axes**).**

Fig 9. PDX screens demonstrate broad combination benefit across multiple MTAP$^{-/-}$ indications

A The dual inhibition of MAT2A and PRMT5 produces deep regressions in MTAP$^{-/-}$ PDX models



B The dual inhibition of MAT2A and PRMT5 produces durable tumor regressions in MTAP$^{-/-}$ PDX models



A) PDX combination efficacy study in 20 MTAP$^{-/-}$ models. Compounds were administered orally once daily at 10 mg/kg (IDE397) or 30 mg/kg (AMG 193). Study duration was up to 98 days. Median response was calculated on the treatment day when either monotherapy reached maximal tumor volume, or on the planned study endpoint (median duration was 57 days, n=5 per group). Negative values denote tumor regressions. **B)** Tumor growth curves of individual mice from the vehicle and IDE397/AMG 193 combination arms. Tumor volume was measured twice weekly.

Conclusions

1. The IDE397/AMG 193 combination maximizes MTA-specific PRMT5 pathway suppression.
2. MAT2A inhibition additionally exploits the metabolic liabilities of MTAP loss for SAM requirements beyond PRMT5.
3. Tumors can adapt to strong and persistent PRMT5 pathway suppression via bypass mechanisms that are prevented by allosteric inhibition of MAT2A. These may include MYC pathway activation and epigenetic reprograming via focused DNA and histone methylation events.
4. IDE397/AMG 193 combination therapy strongly constrains biological avenues for monotherapy drug adaptation; thus, delivering durable antitumor activity.

Acknowledgements

The authors would like to acknowledge present and former IDEAYA colleagues for their many contributions to the scientific and clinical enterprise; and our CRO and industry partners who have contributed to the nonclinical studies: DepMap Consortium, Eurofins, Proteros, Promega, Pharmaron, Xentech, Champions, Charles River Laboratories-Freiburg, HistoWiz, Horizon Discovery, Discovery Life Sciences, FIOS Genomics, ActiveMotif, Sapient Bio, and Cellecta.

References

1. Belmontes, B. et al. 2024 *Cancer Discovery*
2. Rothweiler, EM. et al. 2024 *BioRxiv*
3. Trincado, JL. et al. 2018 *Genome Biol*
4. Drew A, et al., 2017 *Sci Rep*
5. Nakayama K, et al., 2018 *Oncotarget*